ACCOUNTS
of chemical research

Self-Assembling Organic Nanotubes with Precisely Defined, Sub-nanometer Pores: Formation and Mass Transport Characteristics

BING GONG*,†,‡ AND ZHIFENG SHAO*,§

†Department of Chemistry, University at Buffalo, The State University of New York, Buffalo, New York 14260, United States, ‡College of Chemistry, Beijing Normal University, Beijing 100875, China, and §Key Laboratory of Systems Biomedicine, State Key Laboratory for Oncogenes & Related Genes and School of Biomedical Engineering, Shanghai Jiao Tong University, Shanghai 200240, China

RECEIVED ON JANUARY 31, 2013

CONSPECTUS

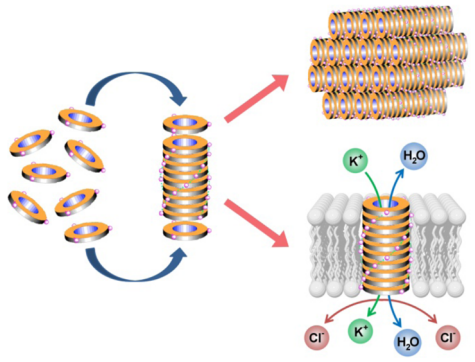

The transport of molecules and ions across nanometer-scaled pores, created by natural or artificial molecules, is a phenomenon of both fundamental and practical significance. Biological channels are the most remarkable examples of mass transport across membranes and demonstrate nearly exclusive selectivity and high efficiency with a diverse collection of molecules. These channels are critical for many basic biological functions, such as membrane potential, signal transduction, and osmotic homeostasis.

If such highly specific and efficient mass transport or separation could be achieved with artificial nanostructures under controlled conditions, they could create revolutionary technologies in a variety of areas. For this reason, investigators from diverse disciplines have vigorously studied small nondeformable nanopores. The most exciting studies have focused on carbon nanotubes (CNTs), which have exhibited fast mass transport and high ion selectivity despite their very simple structure. However, the limitations of CNTs and the dearth of other small ($\leq$2 nm) nanopores have severely hampered the systematic investigation of nanopore-mediated mass transport, which will be essential for designing artificial nanopores with desired functions en masse.

Researchers can overcome the difficulties associated with CNT and other artificial pores by stacking macrocyclic building blocks with persistent shapes to construct tunable, self-assembling organic pores. This effort started when we discovered a highly efficient, one-pot macrocyclization process to efficiently prepare several classes of macrocycles with rigid backbones containing nondeformable cavities. Such macrocycles, if stacked atop one another, should lead to nanotubular assemblies with defined inner pores determined by their constituent macrocycles. One class of macrocycles with aromatic oligoamide backbones had a very high propensity for directional assembly, forming nanotubular structures containing nanometer and sub-nanometer hydrophilic pores. These self-assembling hydrophilic pores can form ion channels in lipid membranes with very large ion conductances.

To control the assembly, we have further introduced multiple hydrogen-bonding side chains to enforce the stacking of rigid macrocycles into self-assembling nanotubes. This strategy has produced a self-assembling, sub-nanometer hydrophobic pore that not only acted as a transmembrane channel with surprisingly high ion selectivity, but also mediated a significant transmembrane water flux.

The stacking of rigid macrocycles that can be chemically modified in either the lumen or the exterior surface can produce self-assembling organic nanotubes with inner pores of defined sizes. The combination of our approach with the availability and synthetic tunability of various rigid macrocycles should produce a variety of organic nanopores. Such structures would allow researchers to systematically explore mass transport in the sub-nanometer regime. Further advances should lead to novel applications such as biosensing, materials separation, and molecular purifications.

Introduction

Many unusual phenomena have been observed at nanoscopic dimensions, perhaps none more intriguing than what has been found within the confined spaces of nanopores, whether natural or man-made.[1] Among these, the unexpected mass transport properties of these tiny pores

Published on the Web 04/18/2013 www.pubs.acs.org/accounts
10.1021/ar400030e

(with bore diameters down to sub-nanometer dimensions) is creating tremendous excitement not only for what their study has revealed of natural processes at these length scales but also for their potential applications in a wide range of areas, including medicine, chemistry, and industry.

The most sophisticated nanopores made by nature are biological channels that possess extraordinary properties in molecular transport. For instance, potassium ion channels, critically important for the maintenance of cell membrane potential,[2] exhibit a selectivity of potassium over sodium that exceeds 10 000.[3] Aquaporins, responsible for osmotic homeostasis of a cell, readily permit a high flux of water molecules even to the exclusion of protons.[4]

Presently the most studied artificial nanopores are those of carbon nanotubes (CNTs) owing to their extraordinary mass transport characteristics. In 2001, results from molecular dynamics (MD) simulations on the 8.1 Å pore of a single-walled CNT suggested that water molecules could spontaneously and continuously fill the sub-nanometer pore as a one-dimensionally ordered chain, with rapid, pulse-like transmission through the highly hydrophobic lumen.[5] This unusual property of hydrophobic nanopores was confirmed experimentally in 2006.[6] The transport of water and methane through aligned CNTs with pores smaller than 2 nm were found to be several orders of magnitude faster than classical theories would have predicted. These early discoveries had prompted intense interest in mass transport through small hydrophobic nanopores. For example, MD simulations demonstrated that sub-nanometer pores with radii in the range of 1.5−6.5 Å selected K^+ over Na^+.[7] Comparing the hydration of K^+ and Na^+ in narrow single-walled CNTs showed that constraining a hydrated K^+ inside narrow (0.60 and 0.73 nm) CNTs was more favorable, while the situation was reversed inside CNTs with larger diameters.[8]

The unique behavior of CNT pores has been attributed to their nondeformability, precisely defined diameters, hydrophobicity, and smooth inner walls, which provide confinement within their nanometer and sub-nanometer size spaces. However, efforts to further characterize the factors responsible for the observed function are impeded by a multitude of obstacles, including the difficulty in tuning the diameters of CNT pores or functionalizing their inner walls. Additionally, the production and purification of CNTs with uniform diameters from 0.4 to 3 nm are nontrivial at the least.

Inspired by the extraordinary properties of biological and CNT pores, a variety of other artificial channels has been designed and explored, with the objective of realizing controllable creation of nanosized pores.[9−15] Among the known examples, however, few could generate nanopores with defined diameters[9,13,14] or with functions suitable for practical applications.[9,13−15] Clearly, controlling the size, surface chemistry, and physical properties of synthetic pores of $\leq$2 nm in size remains a daunting challenge. Creating efficient methodologies that would allow systematic modifications are essential if we were to recapitulate some of the extraordinary properties of biological channels with synthetic nanopores.

With their synthetic modifiability, organic nanotubes should be ideal candidates for overcoming many of the limitations of CNTs and other materials by providing structure−function correlation for the unusual properties and phenomena in the nanometer and sub-nanometer territories. Among known strategies,[16−26] forming nanotubes by stacking cyclic building blocks has allowed the inner and outer diameters, as well as the surface properties of the resultant tubular assemblies, to be encoded by the constituent rings.

One group of macrocycles that have attracted intense interest are those with persistent shapes.[27,28] Prior to our discovery,[29] the majority of rigid macrocycles are those with planar π-conjugated backbones.[30−36] These macrocycles, with rigid, flat backbones and defined diameters, would lead to nanotubes with inner pores of defined diameters if stacked atop one another. If a reliable ring-stacking strategy is achieved, synthetically modifying the macrocyclic building blocks should allow the size and property of the self-assembled pore to be tuned. Furthermore, the rigidity of such macrocycles may allow the placement of functional groups at defined locations, something that is very difficult to realize with CNT and inorganic pores.

Our interest in organic nanopores originated from our effort in developing cavity- and pore-containing organic structures, initially based on the folding of unnatural oligomers[37] and more recently by controlling the stacking of rigid macrocyles.[38] Rigidifying the backbones of oligomers consisting of rigid planar residues connected via planar linkages such as amide or urea groups with localized intramolecular hydrogen bonds led to the creation of stably folded oligomers that adopt crescent and helical conformations containing well-defined internal cavities.[39] Subsequent extension of the enforced folding approach resulted in the discovery of a highly efficient, one-pot macrocyclization process that has opened a new avenue for the efficient preparation of several new classes of rigid cavity-containing macrocyles.[29,40,41] Our recent effort in creating higher-order

SCHEME 1

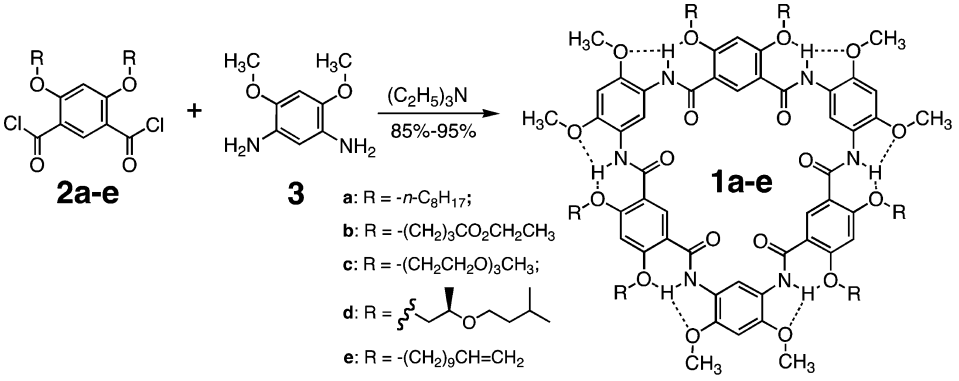

structures based on rigid macrocycles has led to tubular structures containing pores with uniform sub-nanometer diameters.[42,43]

This Account focuses on our efforts in (1) developing rigid macrocyclic molecular building blocks, (2) assembling of rigid macrocycles into tubular noncollapsible sub-nanometer organic pores, and (3) characterizing ion and molecular transport mediated by the organic pores. In recent years, a number of porous synthetic structures have been reported,[17,22,44−53] many of which possess interesting mass transport properties. Due to space limit, these systems are not discussed in this Account. Interested readers may consult several excellent reviews published recently.[54−56]

Rigid Macrocyclic Building Blocks

One-Step, Highly Efficient Synthesis of Aromatic Oligoamide Macrocycles. Our efforts in developing porous foldamers[37] based on the enforced folding of unnatural oligomers have led to a series of aromatic oligoamides that adopt stable crescent or helical conformations containing cavities of 10−30 Å across.[37] In 2004, an attempt to extend the same folding principles to the preparation of folding polymers led to the discovery of highly efficient (>80% yields), one-pot formation of a series of oligoamide macrocycles (Scheme 1).[29] Instead of forming the expected polyamide chains, treating diacid chlorides **2a**−**e** with diamine **3** led to macrocycles **1a**−**e** in very high yields. Macrocycles **1a**−**e** have a nearly flat persistent shape and a noncollapsible hydrophilic cavity of ∼8.5 Å.

A Folding-Assisted Cyclization Mechanism. This one-pot process represents an unprecedented example of kinetic macrocyclization. The nearly exclusive formation of macrocycles **1** and the dearth of byproducts contrast sharply to what had been known about kinetic macrocyclization. Due to irreversible bond formation, kinetic macrocyclization is known to be invariably accompanied by "overshooting" byproducts, resulting in poor yields of desired macrocycle(s).[30] Our subsequent study[40] revealed a unique mechanism. We found that, due to the folding of oligoamide precursors, uncyclized oligomers with lengths shorter than or the same as that of a target macrocycle are favorably formed, while formation of longer uncyclized oligomers that would lead to undesired products is hampered by a "remote steric effect".[40]

One-Pot Formation of Rigid Oligoamide Macrocycles with Expanded Cavities[40]. This folding-assisted mechanism predicts that, other macrocycles should also form efficiently if their oligomeric precursors adopt rigid crescent conformations. For example, when *para*-linked residues are introduced, the backbone curvature is reduced, resulting in enlarged cavities. Similar to **1**, *para*-diacid chloride **7** and *meta*-diamines **8a**−**d** were reacted in one pot (Scheme 2). Analyzing the crude products by MALDI-TOF revealed three sets of major peaks corresponding to the molecular ions of the 14-, 16-, and 18-residue macrocycles **4**, **5**, and **6**. With different side chains, the relative peak intensities corresponding to the three macrocycles remain nearly the same, being roughly **5** > **4** > **6** with a combined yield of over 80%. After being separated with flash column chromatography, the yields of macrocycles **4c**, **5c**, and **6c** were determined to be 24%, 37%, and 9.2%, respectively. The highly symmetric cyclic structures of these macrocycles were confirmed by their ^{1}H NMR spectra. The cavities of **4**−**6**, being 2.3, 2.6, and 3.0 nm across, are greatly expanded in comparison to that of **1a**−**d**.

The formation of three, instead of one, macrocycles from the reactions of **7** and **8** was explained by the small variability of amide bond angles. The oligomeric precursors of **4**−**6**, which consist of *meta*/*para*-linked residues, require more residues and amide bonds than those of **1** to place their two reactive termini into a "cyclizable" range. The flexibility of amide bond angles means that multiple

SCHEME 2

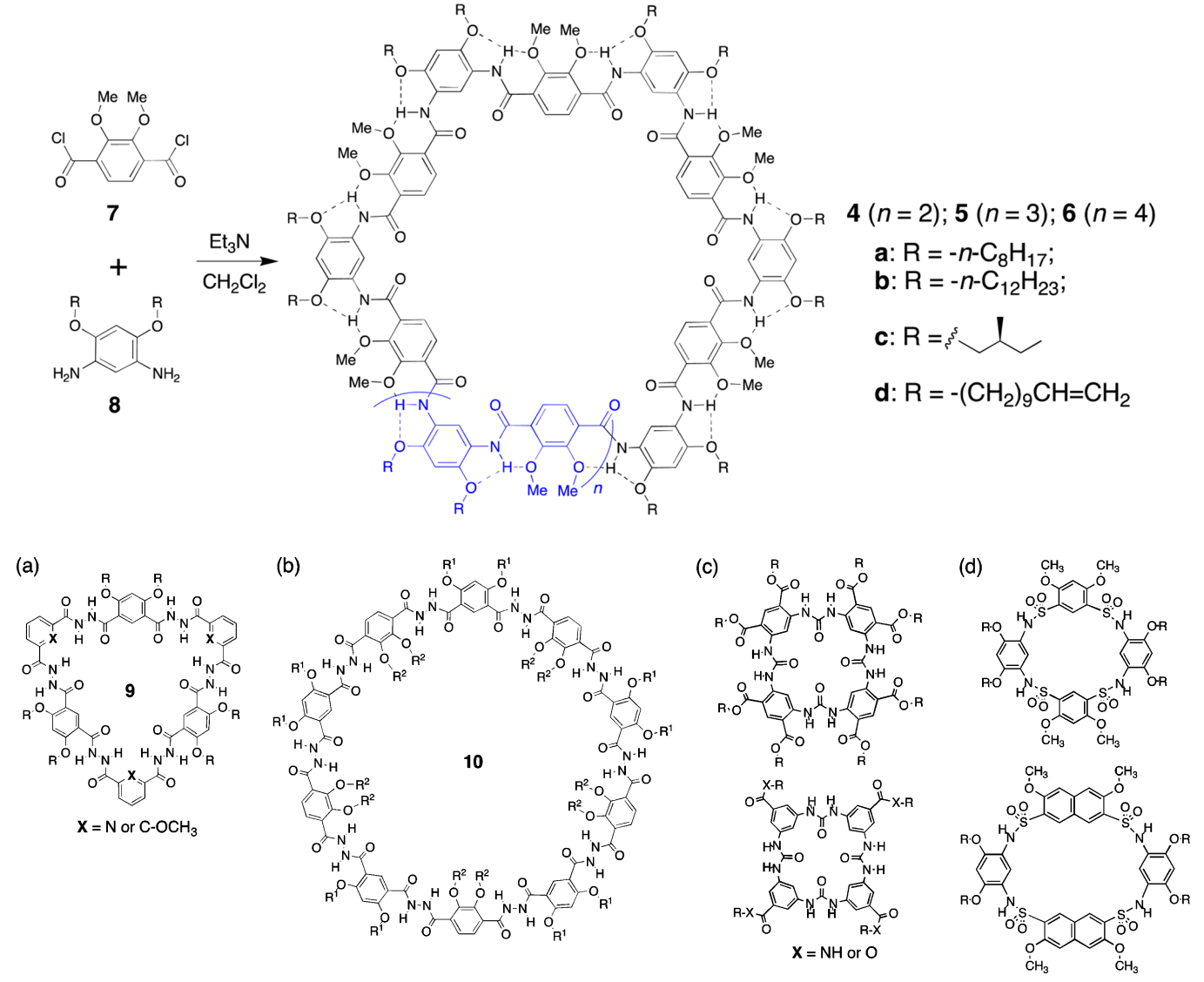

FIGURE 1. Shape-persistent macrocycles with aromatic oligohydrazide (a, b), oligourea (c), and sulfonamide backbones (d).

oligomers, in this case the 14-, 16-, or 18-mer, could all fall into such a cyclizable range. Further modifying the one-pot strategy by reacting *para*-diacid chloride **7** with a trimeric or pentameric diamine led to the formation of the 16-residue **5** or the 18-residue **6** with over 80% yields while preventing the other macrocycles from forming.

Other Rigid Macrocycles Prepared in Recent Years. The folding-assisted mechanism has also enabled the preparation of other rigid macrocycles. For example, macrocycles **9** and **10** were prepared in high (up to 97%) yields from the one-pot reaction of monomeric diacid chlorides and dihydrazides (Figure 1a,b).[41] Macrocycles **9** and **10** have hydrogen bond-rigidified planar backbones with internal cavities ranging from 10 to 25 Å across. A unique feature of these macrocycles is their inward-pointing (X or R^2) groups in the cavities, amenable to further modifications.

We have also discovered other rigid macrocycles with backbones consisting of aromatic residues connected by urea (Figure 1c),[57] sulfonamide (Figure 1d),[58] and sulfonate[59] linkages. These discoveries, as summarized in a recent review,[38] have greatly expanded the inventory of readily available shape-persistent macrocycles.

Self-Assembly of Rigid Macrocycles: Nanotubes Containing Internal Pores with Precisely Defined Diameters

Tubular Assembly of Cyclic Oligoamides[42]. When macrocycles **1** were discovered, one of the first observations

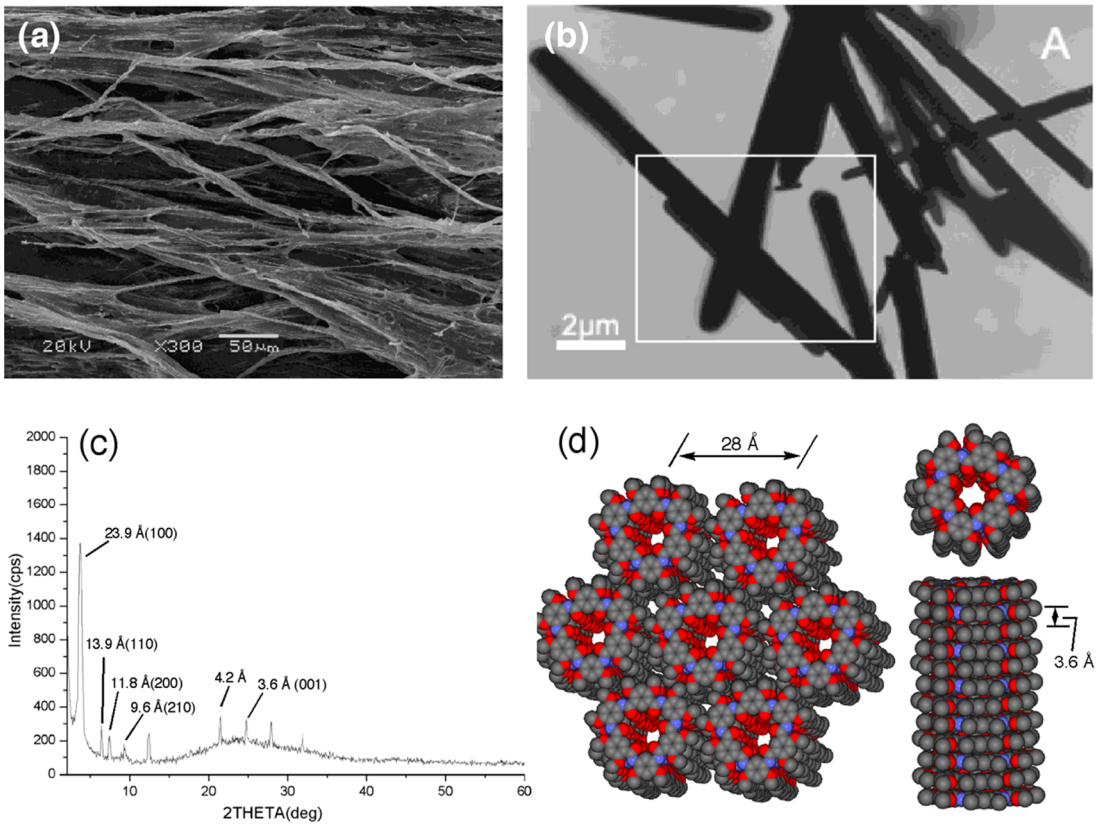

FIGURE 2. (a) The SEM and (b) TEM images and (c) diffractogram of the solid samples of **1e**, prepared by evaporation of solvent, reveal *d* spacings consistent with the columnar packing of **1e** into the hexagonal lattice (d).

made on them was their highly broadened ^{1}H NMR signals in chloroform, especially those of the aromatic protons. Under conditions such as elevated temperature or the presence of a polar solvent, ^{1}H NMR spectra with improved resolution could be obtained. This phenomenon can be attributed to the aggregation of these macrocycles. Dynamic light scattering (DLS) indicated that macrocycle **1e** (Figure 2), bearing six highly solubilizing alkenyl side chains, formed large aggregates with average sizes dependent on concentration, temperature, and solvents. Consistent with ^{1}H NMR results, aggregate size decreased in polar solvents. For example, in sharp contrast to the large aggregates (average size 1909 nm) formed by **1e** (5 mM) in chloroform, the aggregates formed in acetone at the same concentration were 10-fold smaller, and only molecularly dissolved (monomeric) **1e** exists in DMF. Thus, the aggregation of **1e** was proportionally weakened as solvent polarity increased. This observation seemed to contrast with what is known about the stacking of aromatic molecules, that is, $\pi-\pi$ stacking is promoted in polar solvents and discouraged in nonpolar solvents.[60]

The directional aggregation of **1e** in the solid state was shown by images from scanning electron microscopy (SEM) and transmission electron microscopy (TEM), which revealed the presence of long fibers (Figure 2a) or straight, rod-like assemblies (Figure 2b). Strong directional assembly is not limited to **1**, and the 16-residue **5d** also formed straight, rod-like assemblies.[42] These results suggest that highly directional assembly is a common phenomenon associated with this series of oligoamide macrocycles.

Details on the packing of **1e** in the solid state were provided by X-ray diffraction (XRD), which revealed a pattern that contains sharp reflections typical of columns packed on a hexagonal lattice (Figure 2c). A lattice parameter of 27.6 Å, consistent the diameter of **1e**, suggests that the macrocycles stack into columns (or tubes) that undergo further hexagonal packing (Figure 2d). A sharp peak at 3.60 Å, typical of $\pi-\pi$ stacking, corresponds to a correlation length of 69.6 nm based on Scherrer's equation.[42] This indicates that ~193 macrocycles continuously stacked into a nanotube. XRD study also revealed columnar stacking and further hexagonal packing for **5d**, suggesting that oligoamide macrocycles of different sizes have a high propensity for tubular assembly.

It was found that the rod-like fibers formed by **1e** and the columnar and hexagonal packing of **1e** did not change with

added Cs^+ salt, which suggests the presence of a hydrophilic inner pore of >8 Å that is defined by the cavity of stacked macrocycles.

Hydrogen Bond-Directed Tubular Assembly of Shape-Persistent Macrocycles[43]. At the time when we noticed the strong directional assembly of oligoamide macrocycles, we also started to develop a strategy for controlling the columnar stacking of rigid macrocycles that otherwise are reluctant to self-superpose. Our approach involved equipping hexakis(*m*-pheneylene ethylene) (*m*-PE) macrocycles with multiple hydrogen-bonding side chains. Specifically, *m*-PE macrocycles **11a** and **11b** (Figure 3a), each carrying six secondary amide side chains, were designed. These two *m*-PE macrocycles were chosen because analogous macrocycles that associate solely via $\pi-\pi$ stacking tend to have a poor tendency to align into tubular assemblies.[19,20] It was reasoned that to engage in maximum hydrogen-bonding interactions, two such cyclic molecules have to stack in a superposed fashion, leading to the alignment of their backbones and their internal cavities. Repeating this stacking mode with additional cyclic molecules would lead to a hydrogen-bonded stack.

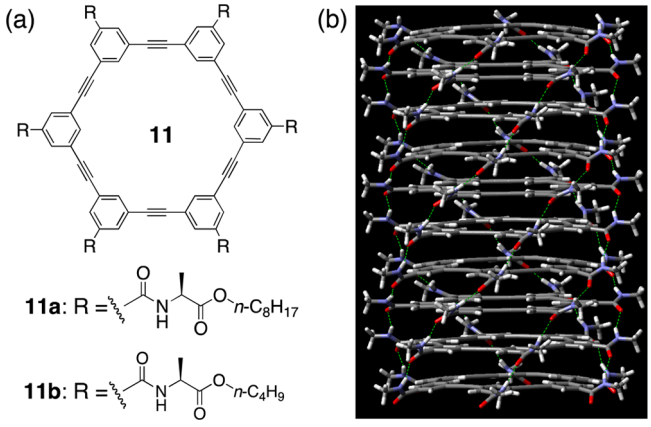

FIGURE 3. (a) Structures of *m*-PE macrocycles **11a** and **11b** that bear multiple hydrogen-bonding (amide) side chains. (b) A helical nanotubular assembly consisting of **11** (R replaced with $CONHCH_3$) optimized using a periodic density functional theory method and basis set (HCTH407/DND), implemented in DMol3 software package.

Ab initio optimization of a tubular stack consisting of **11** (replacing R of **11a** or **11b** with $CONHCH_3$) revealed a *helical tube* in which the macrocycles underwent relative rotation to satisfy the optimal distances of both side chain hydrogen bonding and backbone stacking (Figure 3b).

In contrast to the often challenging fabrication of 1D assemblies from disc-like molecules, samples of **11a** and **11b** prepared under a variety of conditions, including solution dispersion, phase transfer, or vapor diffusion, all led to long fibers, which demonstrates the high propensity of these macrocycles to undergo anisotropic aggregation. AFM images of the samples of **11a** (Figure 4a) or **11b** (Figure 4b) showed nanofilaments having a diameter (37 ± 0.2 Å for **11a** or 32 ± 1 Å for **11b**) consistent with that of the macrocycle, suggesting that the macrocycles indeed superposed into tubes (Figure 4c).

In solution, the aggregation of **11a** or **11b** was probed by using DLS, UV−vis, fluorescence, and circular dichroism (CD) spectroscopy. DLS indicated that **11a** (1 mg/mL in CCl_4) formed aggregates with an average size distribution of 433 nm. The CD spectra of **11a** in CCl_4 revealed strong Cotton effect near the λ_{max} (~270 nm) of the backbone chromophore, revealing the presence of chiral supramolecular assemblies (Figure 5a), which is very similar to that recorded in solution (Figure 5a) and as thin films (Figure 5b). The chirality of the tubular structure as indicated by CD spectra can only be explained by the formation of a left- or

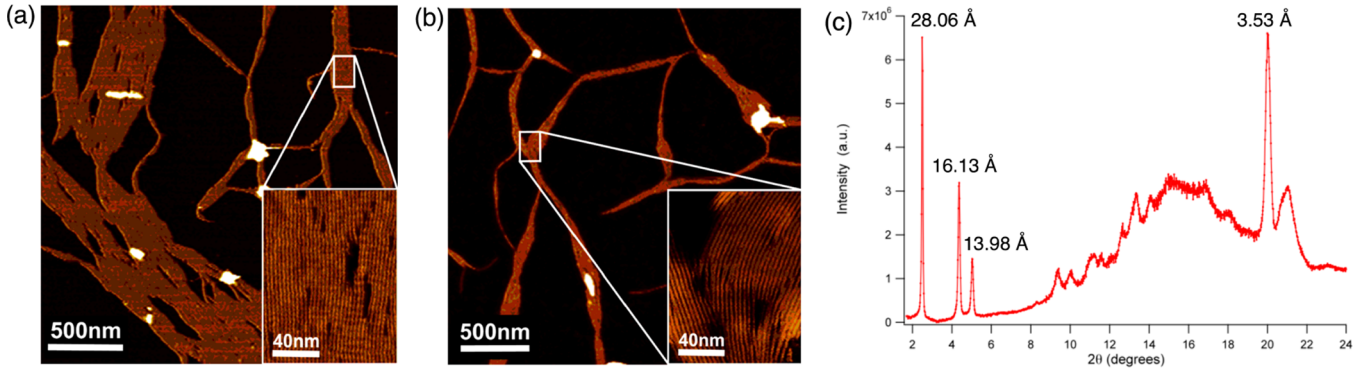

FIGURE 4. AFM image of a sample of (a) **11a** and (b) **11b**. Insets show uniform nanofilaments closely packed into quasi-parallel aggregates revealed at higher resolution. (c) XRD reveals that the tubes formed by **11b** packed in a 2D hexagonal lattice at an intertube distance of 32 Å in agreement with the diameter determined by AFM.

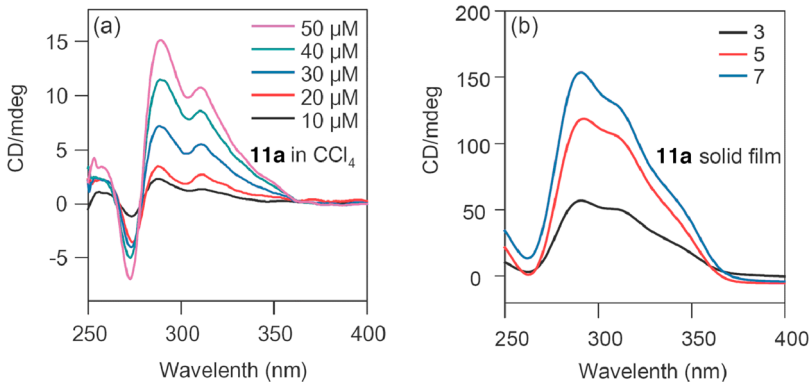

FIGURE 5. The CD spectra of (a) **11a** in CCl_4 measured at room temperature and (b) thin films of **11a** formed by depositing three, five, and seven layers of a 0.5 mM solution in CCl_4 on quartz.

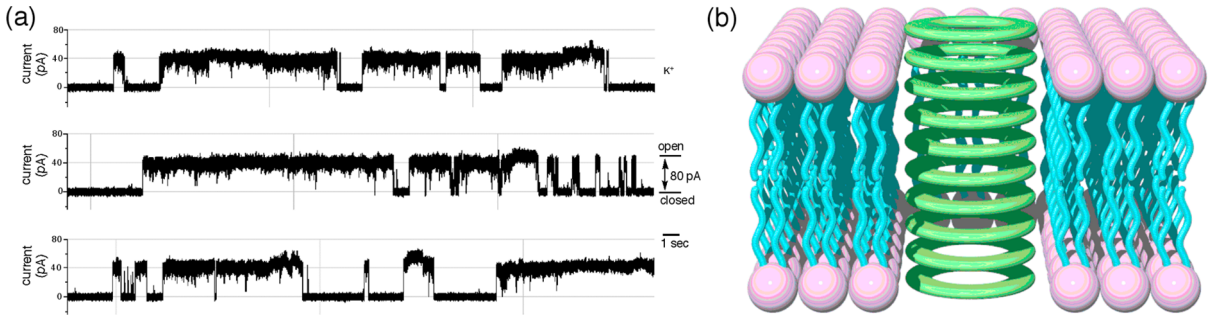

FIGURE 6. (a) A 108-s continuous K^+ single channel conductance recording at 50 mV with **1d** (0.32 μM). (b) Based on the conductance of **1d**, a tubular structure consisting of stacked macrocyclic molecules was proposed to act as a transmembrane channel.

right-handed helical nanotube. The handedness is biased due to the presence of chiral side chains. These studies have clearly demonstrated that rigid *m*-PE macrocycles can be forced to stack into well-defined helical nanotubes by multiple hydrogen bonds. Such a controlled self-assembling strategy should be of general applicability for aligning flat molecular objects including macrocycles with planar, nondeformable shapes.

Transmembrane Mass Transport Mediated by Self-Assembling Nanopores

Highly Conducting Transmembrane Ion Transport Mediated by Oligoamide Macrocycles.[61]. Given their strong and directional aggregation, hydrophilic lumen, and hydrophobic exterior, we reasoned that macrocycles **1** might assemble into tubular structures inside the hydrophobic core of lipid bilayers and form transmembrane ion channels.

With large unilamellar vesicles (LUVs) encapsulating a pH-sensitive fluorescent dye (HPTS), the addition of **1d** led to a rapid fluorescence quenching of HPTS in a low pH solution, suggesting that **1d** significantly increased the proton permeability of the LUV. Macrocycle **1d** was found to produce an exchange rate constant of $5.65 \pm 1.62\ s^{-1}$ using ^{23}Na NMR shift assay. This is roughly half the value of the well-studied model ion channel formed by gramicidin,[62] which confirms the presence of transmembrane **1d** channels.

However, the most conclusive evidence of well-defined ion channels by **1d** in lipid bilayers came from single-channel recordings. Upon dilution into the aqueous phase, **1d** could apparently partition into the lipid bilayer and exhibited well-defined single-step conductance changes of 770 ± 30 pS in 0.5 M KCl (Figure 6a). Another macrocycle, sharing the same oligoamide backbone as **1d** but with different side chains, also formed a single transmembrane conductance of 890 ± 52 pS (in 0.5 M KCl). The similar conductances observed with these two macrocycles, both of which have the same internal cavity, indicated that ion transport occurs through the cavities of these molecules, that is, the self-assembled pores of the stacked macrocycles. Such a conductance is similar to that of the bacterial toxin, α-hemolysin.[63]

If the pore could be considered as a uniform cylinder, its diameter can be estimated based on Hille's equation.[3] Taking the length as 40 Å, the thickness of a lipid bilayer,

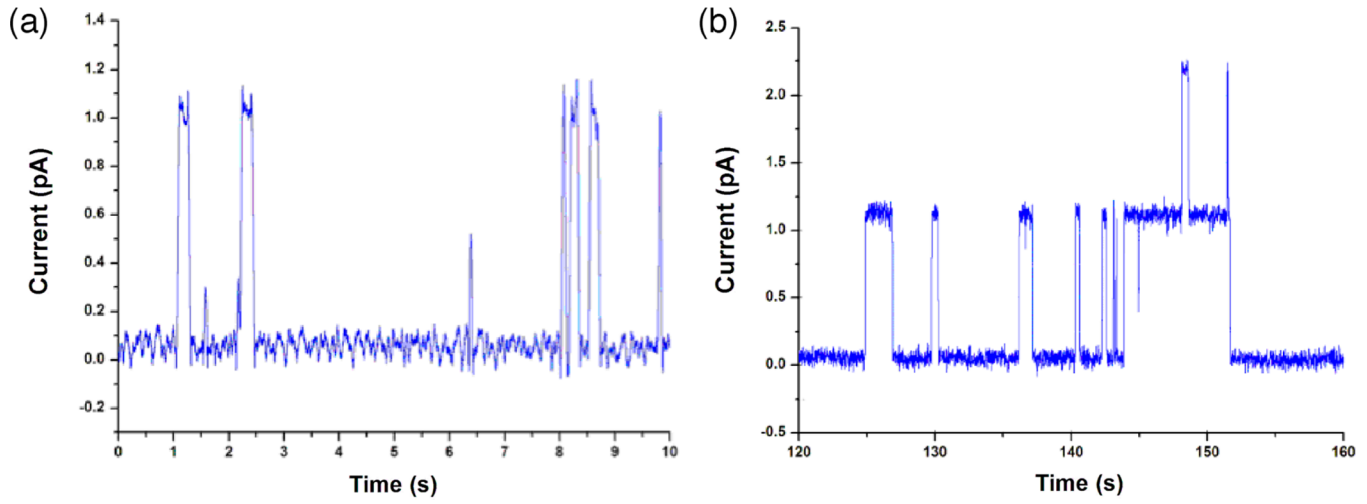

FIGURE 7. (a) A 10-s single channel recording with **11b** (20 μM) at 200 mV in HCl (1 mM) across a planar lipid bilayer. (b) A 40-s trace of single channel recording with **11b** (10 μM) at 200 mV in KCl (4.0 M, pH 6.0).

yields a **1d** pore diameter of 8.5 Å, supporting a model of cofacially stacked macrocycles into nanotubes (Figure 6b). This conclusion is also consistent with the measurements with the analogous **1e** (see Figure 2 above).[42]

Unusual Mass Transport of a Sub-nanometer Hydrophobic Pore[43]. Based on the above success, we expected that, with their hydrophobic side chains, macrocycle **11a** or **11b** could also partition into the hydrophobic core of lipid bilayers and self-assemble into transmembrane nanopores that are hydrophobic. As expected, LUV-based assays clearly demonstrated that **11b** can facilitate rapid proton transport across the lipid bilayer. Single-channel recordings confirmed well-defined conductance steps of ~5 pS in 1 mM HCl (Figure 7a). These channels exhibited a striking proton selectivity over chloride ($P_{H^+}/P_{Cl^-} > 3000$), even higher than that of a protein proton channel, influenza virus M2 protein ($P_{H^+}/P_{Cl^-} = 19.7$).[64] The channel formed by **11b** also showed well-defined currents in 4 M KCl with a mean conductance of ~5.8 pS (Figure 7b). Based on the differences in ion concentration required to obtain these similar conductances, we could infer a proton over potassium permeability ratio of ~2000. The ion selectivity of the structurally simple **11b** nanopore is extraordinary in comparison to other synthetic channels.[65]

The ion conductance of the **11b** channel implies that this hydrophobic pore may be filled with water. To measure water transport, the volume change of liposomes (LUVs) loaded with carboxyfluorescein (CF) must be monitored, by using stopped-flow kinetic measurements (Figure 8a).[66] Because the lipid bilayer is also water-permeable,[67] upon external osmolarity increase, meaningful conclusions about the water transport of the nanopores can only be made by comparing the rate (kinetics) of fluorescence change within a short time period before the system reaches equilibrium, with and without the added compound. As shown in Figure 8b, LUVs with **11b** exhibit a faster decay of fluorescence (blue) than those without (red). The estimated water permeability of a single **11b** channel was calculated to be $(2.6 \pm 0.4) \times 10^{-14}$ cm^3/s when open, about 22% that of AQP1/CHIP-28 (11.7×10^{-14} cm^3/s).[66] Given that the sub-nanometer hydrophobic pore formed by macrocycles **11** has an inner surface that is very different from those of CNTs, unusual mass transporting efficiency and selectivity seem to be a general property associated with sub-nanometer dimensions.

Conclusions and Future Perspective

An initial effort to create cavity-containing molecular structures based on an enforced folding strategy took an unexpected turn upon the discovery of a one-pot macrocyclization process that subsequently resulted in the successful synthesis of many cavity-containing macrocycles with defined shapes. The ready availability of rigid macrocycles, along with their synthetic modification, prompted us to explore and control the assembly of these molecules into higher-level supramolecular structures. The high propensity of our oligoamide macrocycles for spontaneous self-assembly into nanotubes afforded hydrophilic pores of defined sizes, which can in turn serve as highly conductive transmembrane channels. In contrast, the hydrophobic channels formed by the *m*-PE macrocycles, without any further modification, exhibited highly selective ion transport and surprisingly efficient water flux.

We are pleasantly surprised that even without the complicated folding and precisely placed functional groups as in

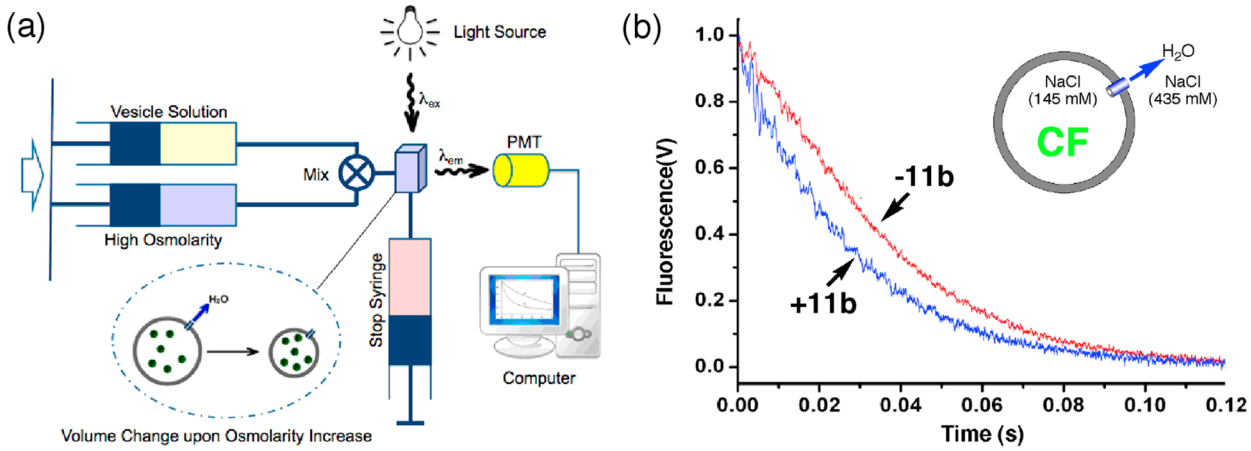

FIGURE 8. (a) Schematic illustration of the stopped-flow kinetic technique. Two solutions, one of LUVs with encapsulated CF in the presence of NaCl at a lower concentration and the other of NaCl at a higher concentration, are rapidly mixed together. The created osmotic gradient across the membrane will drive water out of the vesicles, leading to a decrease of the inner volume of a LUV and thus enhanced fluorescence quenching of the encapsulated CF. (b) Water permeability measured with CF-containing liposomes in the presence (blue) and absence (red) of **11b**. The lipid to **11b** ratio is 50. LUVs were abruptly exposed to a high extravesicular osmolality with a final osmolarity ratio of 3. The increase in the quenching rate indicates the **11b** mediated water permeability.

a typical protein channel, simply by controlling the size and the surface properties of a nanoconfined lumen, some of the most exciting properties of biological channels could be recapitulated with these self-assembled nanopores. Undoubtedly, the ability to incorporate various functional residues inside and outside the nanopore by synthetically modifying the constituent macrocycles should offer countless possibilities to create different nanopores with even more complex and controlled functions that could eventually rival, and perhaps replace, those found in nature. Achieving such a goal could lead to many practical applications such as sensing, separation, and purification of various molecules or even complementing some of the channel functions in clinical medicine in the future.

We would like to thank previous and current students, postdoctoral fellows and collaborators who have made this research possible, and Professor D. M. Czajkowsky for a critical reading of the manuscript. B.G. is supported by the National Science Foundation (Grant CBET-1066947), the Petroleum Research Fund administered by the ACS (Grant 51048-ND7), and the Natural Science Foundation of China (Grant 91227109). Z.S. is supported by the Natural Science Foundation of China (Grants 91027020, 11074168, and 21273148) and Ministry of Science and Technology of China (Grants 2010CB529205 and 2012AA020103).

BIOGRAPHICAL INFORMATION

Bing Gong received his bachelor's degree in chemistry from Sichuan University in China in 1984 and Ph.D. in 1990 from the University of Chicago under the supervision of Professor David Lynn. He then joined the laboratory of Professor Peter Schultz as a Damon Runyon-Walter Winchell Fund Postdoctoral Fellow at the University of California, Berkeley. He began his independent academic career in 1994 and is currently Professor of Chemistry at the State University of New York at Buffalo. In recent years, he has been actively engaged in a research effort in China. His research interests include directed self-assembly, the folding of biomimetic unnatural molecules, and the creation of nanoporous organic structures.

Zhifeng Shao received his bachelor's degree in physics from Nanjing University in China in 1982 and a Ph.D. in 1988 from University of Chicago under the supervision of Professor A. V. Crewe. He then became an assistant professor of molecular physiology and biophysics in 1989 and full professor in 1998 at University of Virginia. He was elected Fellow of AAAS in 2000 and is the K. C. Wong Chair and professor of biomedical engineering at Shanghai Jiao Tong University since 2009. His research interests include self-assembled biomimetic systems, nanoscale structural characterization and functional genomics.

FOOTNOTES

*E-mail addresses: bgong@chem.buffalo.edu; zfshao@sjtu.edu.cn.
The authors declare no competing financial interest.

REFERENCES

1 Bocquet, L.; Charlaix, E. Nanofluidics, from bulk to interfaces. *Chem. Soc. Rev.* **2010**, *39*, 1073–1095.
2 Aidley, D. J. *The Physiology of Excitable Cells*, 4th ed.; Cambridge University Press: Cambridge, U.K., 1998.
3 Hille, B. *Ion Channels of Excitable Membranes*, 3rd ed.; Sinauer: Sunderland, MA, 2001.
4 Agre, P. Aquaporin water channels (nobel lecture). *Angew. Chem., Int. Ed.* **2004**, *43*, 4278–4290.
5 Hummer, G.; Rasaiah, J. C.; Noworyta, J. P. Water conduction through the hydrophobic channel of a carbon nanotube. *Nature* **2001**, *414*, 188–190.
6 Holt, J. K.; Park, H. G.; Wang, Y. M.; Stadermann, M.; Artyukhin, A. B.; Grigoropoulos, C. P.; Noy, A.; Bakajin, O. Fast mass transport through sub-2-nanometer carbon nanotubes. *Science* **2006**, *312*, 1034–1037.

7 Carrillo-Tripp, M.; Saint-Martin, H.; Ortega-Blake, I. Minimalist molecular model for nanopore selectivity. *Phys. Rev. Lett.* **2004**, *93*, No. 168104.

8 Shao, Q.; Zhou, J.; Lu, L. H.; Lu, X. H.; Zhu, Y. D.; Jiang, S. Y. Anomalous hydration shell order of Na^+ and K^+ inside carbon nanotubes. *Nano Lett.* **2009**, *9*, 989–994.

9 Jirage, K. B.; Hulteen, J. C.; Martin, C. R. Nanotubule-based molecular-filtration membranes. *Science* **1997**, *278*, 655–658.

10 Yang, S. Y.; Ryu, I.; Kim, H. Y.; Kim, J. K.; Jang, S. K.; Russell, T. P. Nanoporous membranes with ultrahigh selectivity and flux for the filtration of viruses. *Adv. Mater.* **2006**, *18*, 709–712.

11 Gankema, H.; Hempenius, M. A.; Möller, M.; Johansson, G. Gel template leaching: An approach to functional nanoporous membranes. *Macromol. Symp.* **1996**, *102*, 381–390.

12 Beginn, U.; Zipp, G.; Mourran, A.; Walther, P.; Möller, M. Membranes containing oriented supramolecular transport channels. *Adv. Mater.* **2000**, *12*, 513–516.

13 Czaplewski, K. F.; Hupp, J. T.; Snurr, R. Q. Molecular squares as molecular sieves: Size-selective transport through porous-membrane-supported thin-film materials. *Adv. Mater.* **2001**, *13*, 1895–1897.

14 Yan, X.; Janout, V.; Hsu, J. T.; Regen, S. L. A polymerized calix[6]arene monolayer having gas permeation selectivity that exceeds Knudsen diffusion. *J. Am. Chem. Soc.* **2002**, *124*, 10962–10963.

15 Akthuakul, A.; Salinara, R. F.; Mayes, A. M. Antifouling polymer membranes with subnanometer size selectivity. *Macromolecules* **2004**, *37*, 7663–7668.

16 Bong, D. T.; Clark, T. D.; Granja, J. R.; Ghadiri, M. R. Self-assembling organic nanotubes. *Angew. Chem., Int. Ed.* **2001**, *40*, 988–1011.

17 Baumeister, B.; Sakai, N.; Matile, S. Giant artificial ion channels formed by self-assembled, cationic rigid-rod beta-barrels. *Angew. Chem., Int. Ed.* **2000**, *39*, 1955–1958.

18 Block, M. A. B.; Kaiser, C.; Khan, A.; Hecht, S. Discrete organic nanotubes based on a combination of covalent and non-covalent approaches. *Top. Curr. Chem.* **2005**, *245*, 89–150.

19 Moralez, J. G.; Raez, J.; Yamazaki, T.; Motkuri, R. K.; Kovalenko, A.; Fenniri, H. Helical rosette nanotubes with tunable stability and hierarchy. *J. Am. Chem. Soc.* **2005**, *127*, 8307–8309.

20 Jonkheijm, P.; Miura, A.; Zdanowska, M.; Hoeben, F. J. M.; De Feyter, S.; Schenning, A. P. H. J.; De Schryver, F. C.; Meijer, E. W. pi-conjugated oligo-(p-phenylenevinylene) rosettes and their tubular self-assembly. *Angew. Chem., Int. Ed.* **2004**, *43*, 74–78.

21 Zhou, M. J.; Nemade, P. R.; Lu, X. Y.; Zeng, X. H.; Hatakeyama, E. S.; Noble, R. D.; Gin, D. L. New type of membrane material for water desalination based on a cross-linked bicontinuous cubic lyotropic liquid crystal assembly. *J. Am. Chem. Soc.* **2007**, *129*, 9574–9575.

22 Percec, V.; Dulcey, A. E.; Balagurusamy, V. S. K.; Miura, Y.; Smidrkal, J.; Peterca, M.; Nummelin, S.; Edlund, U.; Hudson, S. D.; Heiney, P. A.; Hu, D. A.; Magonov, S. N.; Vinogradov, S. A. Self-assembly of amphiphilic dendritic dipeptides into helical pores. *Nature* **2004**, *430*, 764–768.

23 Schnur, J. M. Lipid tubules - A paradigm for molecularly engineered structures. *Science* **1993**, *262*, 1669–1676.

24 Ghadiri, M. R.; Granja, J. R.; Milligan, R. A.; McRee, D. E.; Khazanovich, N. Self-assembling organic nanotubes based on a cyclic peptide architecture. *Nature* **1993**, *366*, 324–327.

25 Seebach, D.; Matthews, J. L.; Meden, A.; Wessels, T.; Baerlocher, C.; McCusker, L. B. Cyclo-beta-peptides: Structure and tubular stacking of cyclic tetramers of 3-aminobutanoic acid as determined from powder diffraction data. *Helv. Chim. Acta* **1997**, *80*, 173–182.

26 Gattuso, G.; Menzer, S.; Nepogodiev, S. A.; Stoddart, J. F.; Williams, D. J. Carbohydrate nanotubes. *Angew. Chem., Int. Ed.* **1997**, *36*, 1451–1454.

27 Moore, J. S. Shape-persistent molecular architectures of nanoscale dimension. *Acc. Chem. Res.* **1997**, *30*, 402–413.

28 Haley, M. M.; Pak, J. J.; Brand, S. C. Macrocyclic oligo(phenylacetylenes) and oligo-(phenyldiacetylenes). *Top. Curr. Chem.* **1999**, *201*, 81–130.

29 Yuan, L. H.; Feng, W.; Yamato, K.; Sanford, A. R.; Xu, D. G.; Guo, H.; Gong, B. Highly efficient, one-step macrocyclizations assisted by backbone-preorganization. *J. Am. Chem. Soc.* **2004**, *126*, 11120–11121.

30 Zhao, D. H.; Moore, J. S. Shape-persistent arylene ethynylene macrocycles: Syntheses and supramolecular chemistry. *Chem. Commun.* **2003**, 807–818.

31 Höger, S. Shape-persistent macrocycles: From molecules to materials. *Chem.—Eur. J.* **2004**, *10*, 1320–1329.

32 Grave, C.; Schlüter, A. D. Shape-persistent, nano-sized macrocycles. *Eur. J. Org. Chem.* **2002**, 3075–3098.

33 Bunz, U. H. F.; Rubin, Y.; Tobe, Y. Polyethynylated cyclic pi-systems: Scaffoldings for novel two and three-dimensional carbon networks. *Chem. Soc. Rev.* **1999**, *28*, 107–119.

34 Gallant, A. J.; MacLachlan, M. J. Ion-induced tubular assembly of conjugated Schiff-base macrocycles. *Angew. Chem., Int. Ed.* **2003**, *42*, 5307.

35 Seo, S. H.; Chang, J. Y.; Tew, G. N. Self-assembled vesicles from an amphiphilic ortho-phenylene ethynylene macrocycle. *Angew. Chem., Int. Ed.* **2006**, *45*, 7526–7530.

36 Zhang, C.-X.; Wang, Q.; Long, H.; Zhang, W. A highly c70-selective shape-persistent rectangular prism constructed through one-step alkyne metathesis. *J. Am. Chem. Soc.* **2011**, *133*, 20995–21001.

37 Gong, B. Hollow crescents, helices and macrocycles from enforced folding and folding-assisted macrocyclization. *Acc. Chem. Res.* **2008**, *41*, 1376–1386.

38 Yamato, K.; Kline, M.; Gong, B. Cavity-containing, backbone-rigidified foldamers and macrocycles. *Chem. Commun.* **2012**, *48*, 12142–12158.

39 Gong, B.; Zeng, H. Q.; Zhu, J.; Yuan, L. H.; Han, Y. H.; Cheng, S. Z.; Furukawa, M.; Parra, R. D.; Kovalevsky, A. Y.; Mills, J. L.; Skrzypczak-Jankun, E.; Martinovic, S.; Smith, R. D.; Zheng, C.; Szyperski, T.; Zeng, X. C. Creating nanocavities of tunable sizes: Hollow helices. *Proc. Natl. Acad. Sci. U. S. A.* **2002**, *99*, 11583–11588.

40 Feng, W.; Yamato, K.; Yang, L. Q.; Ferguson, J.; Zhong, L. J.; Zou, S. L.; Yuan, L. H.; Zeng, X. C.; Gong, B. Efficient kinetic macrocyclization. *J. Am. Chem. Soc.* **2009**, *131*, 2629–2637.

41 Ferguson, J. S.; Yamato, K.; Liu, R.; He, L.; Zeng, X. C.; Gong, B. One-pot formation of large macrocycles with modifiable peripheries and internal cavities. *Angew. Chem., Int. Ed.* **2009**, *48*, 3150–3154.

42 Yang, Y. A.; Feng, W.; Hu, J. C.; Zou, S. L.; Gao, R. Z.; Yamato, K.; Kline, M.; Cai, Z. H.; Gao, Y.; Wang, Y. B.; Li, Y. B.; Yang, Y. L.; Yuan, L. H.; Zeng, X. C.; Gong, B. Strong aggregation and directional assembly of aromatic oligoamide macrocycles. *J. Am. Chem. Soc.* **2011**, *133*, 18590–18593.

43 Zhou, X. B.; Liu, G. D.; Yamato, K.; Shen, Y.; Cheng, R. X.; Wei, X. X.; Bai, W. L.; Gao, Y.; Li, H.; Liu, Y.; Liu, F. T.; Czajkowsky, D. M.; Wang, J. F.; Dabney, M. J.; Cai, Z. H.; Hu, J.; Bright, F. V.; He, L.; Zeng, X. C.; Shao, Z. F.; Gong, B. Self-assembling sub-nanometer pores with unusual mass-transporting properties. *Nature Commun.* **2012**, *3*, No. 949.

44 Lear, J. D.; Wasserman, Z. R.; DeGrado, W. F. Synthetic amphiphilic peptide models for protein ion channels. *Science* **1988**, *240*, 1177–1181.

45 Kubik, S. Large increase in cation binding affinity of artificial cyclopeptide receptors by an allosteric effect. *J. Am. Chem. Soc.* **1999**, *121*, 5846–5855.

46 Tanaka, Y.; Kobuke, Y.; Sokabe, M. A. Nonpeptidic ion-channel with K^+ selectivity. *Angew. Chem., Int. Ed.* **1995**, *34*, 693–694.

47 Cazacu, A.; Tong, C.; van der Lee, A.; Fyles, T. M.; Barboiu, M. Columnar self-assembled ureido crown ethers: An example of ion-channel organization in lipid bilayers. *J. Am. Chem. Soc.* **2006**, *128*, 9541–9548.

48 Ma, L.; Melegari, M.; Colombini, M.; Davis, J. T. Large and stable transmembrane pores from guanosine−bile acid conjugates. *J. Am. Chem. Soc.* **2008**, *130*, 2938–2939.

49 Liu, P.; Ni, R.; Mehta, A. K.; Childers, W. S.; Lakdawala, A.; Pingali, S. V.; Thiyagarajan, P.; Lynn, D. G. Nucleobase-directed amyloid nanotube self-assembly. *J. Am. Chem. Soc.* **2008**, *130*, 16867–16869.

50 Negin, S.; Daschbach, M. M.; Kulikov, O. V.; Rath, N.; Gokel, G. W. Pore formation in phospholipid bilayers by branched-chain pyrogallol[4]arenes. *J. Am. Chem. Soc.* **2011**, *133*, 3234–3237.

51 Kaucher, M. S.; Peterca, M.; Dulcey, A. E.; Kim, A. J.; Vinogradov, S. A.; Hammer, D. A.; Heiney, P. A.; Percec, V. Selective transport of water mediated by porous dendritic dipeptides. *J. Am. Chem. Soc.* **2007**, *129*, 11698–11699.

52 Jeon, Y. J.; Kim, H.; Jon, S.; Selvapalam, N.; Oh, D. H.; Seo, I.; Park, C. S.; Jung, S. R.; Koh, D. S.; Kim, K. Artificial ion channel formed by cucurbit[n]uril derivatives with a carbonyl group fringed portal reminiscent of the selectivity filter of K^+ channels. *J. Am. Chem. Soc.* **2007**, *129*, 11698–11699.

53 Si, W.; Chen, L.; Hu, X. B.; Tang, G. F.; Chen, Z. X.; Hou, J. L.; Li, Z. T. Selective artificial transmembrane channels for protons by formation of water wires. *Angew. Chem., Int. Ed.* **2011**, *50*, 12564–12568.

54 Matile, S.; Jentzsch, A. V.; Montenegro, J.; Fin, A. Recent synthetic transport systems. *Chem. Soc. Rev.* **2011**, *40*, 2453–2474.

55 Chui, J. K.; Fyles, T. M. Ionic conductance of synthetic channels: Analysis, lessons, and recommendations. *Chem. Soc. Rev.* **2012**, *41*, 148–175.

56 Negin, S.; Smith, B. A.; Unger, A.; Leevy, W. M.; Gokel, G. W. Hydraphiles: A rigorously studied class of synthetic channel compounds with in vivo activity. *Int. J. Biomed. Imaging* **2013**, *2013*, No. 803579.

57 Wu, Z. H.; Hu, T.; He, L.; Gong, B. One-pot formation of aromatic tetraurea macrocycles. *Org. Lett.* **2012**, *14*, 2504–2507.

58 He, L.; An, Y.; Yuan, L. H.; Feng, W.; Li, M. F.; Zhang, D. C.; Yamato, K.; Zheng, C.; Zeng, X. C.; Gong, B. Cavity-containing macrocyclic aromatic tetrasulfonamides based on a well-defined structural motif. *Proc. Natl. Acad. Sci. U. S. A.* **2006**, *103*, 10850–10855.

59 Geng, M. W.; Zhang, D. C.; Wu, X. X.; He, L.; Gong, B. One-pot formation and characterization of macrocyclic aromatic tetrasulfonates. *Org. Lett.* **2009**, *11*, 923–926.

60 Smithrud, D. B.; Diederich, F. Strength of molecular complexation of apolar solutes in water and in organic solvents is predictable by linear free energy relationships: A general model for solvation effects on apolar binding. *J. Am. Chem. Soc.* **1990**, *112*, 339–343.

61 Helsel, A. J.; Brown, A. L.; Yamato, K.; Feng, W.; Yuan, L. H.; Clements, A.; Harding, S. V.; Szabo, G.; Shao, Z. F.; Gong, B. Highly conducting transmembrane pores formed by aromatic oligoamide macrocycles. *J. Am. Chem. Soc.* **2008**, *130*, 15784–15785.

62 Urry, D. W. The gramicidin A transmembrane channel: A proposed $\pi_{(L,D)}$ helix. *Proc. Natl. Acad. Sci. U. S. A.* **1971**, *62*, 672–676.

63 Kasianowicz, J. J.; Eric Brandin, E.; Branton, D.; Deamer, D. W. Characterization of individual polynucleotide molecules using a membrane channel. *Proc. Natl. Acad. Sci. U. S. A.* **2006**, *93*, 13770–13773.

64 Vijayvergiya, V.; Wilson, R.; Chorak, A.; Gao, P. F.; Cross, T. A.; Busat, H. D. D. Proton conductance of influenza virus M2 protein in planar lipid bilayers. *Biophys. J.* **2004**, *87*, 1697–1704.

65 Sakai, N.; Matile, S. The determination of the ion selectivity of synthetic ion channels and pores in vesicles. *J. Phys. Org. Chem.* **2006**, *19*, 452–460.

66 Zeidel, M. L.; Ambudkar, S. V.; Smith, B. L.; Agre, P. Reconstitution of functional water channels in liposomes containing purified red cell chip28 protein. *Biochemistry* **1992**, *31*, 7436–7440.

67 Deamer, D. W.; Nichols, J. W. Proton-hydroxide permeability of liposomes. *Proc. Natl. Acad. Sci. U. S. A.* **1983**, *80*, 165–168.